BNL 18057

Conf-730464--1

NEUTRON SCATTERING STUDIES OF SOFT MODE DYNAMICS*

J. D. Axe, S. M. Shapiro, and G. Shirane

Brookhaven National Laboratory

Upton, New York 11973 U. S. A.

T. Riste

Research Establishment, Kjeller, Norway

At the NATO Advanced Study Institute held at nearby Geilo in April 1971, Riste, Samuelsen, and Otnes[1] reported on the critical behavior of $SrTiO_3$ near the 105°K structural phase transformation as studied by neutron scattering. They observed that in addition to the expected condensing soft mode phonon side bands that there was in addition a very narrow central component. This paper is in the nature of a progress report on the neutron scattering work of the last two years on the "central mode problem."

β-TUNGSTEN SUPERCONDUCTORS

The first thing we learned was that the central mode was not an isolated phenomenon occurring only in $SrTiO_3$. At about the same time, Shirane and I were studying the structural transformation in Nb_3Sn.[2] This structural transformation, which occurs in many binary or pseudobinary compounds with the same β-tungsten structure, is characterized by a drastic softening of the acoustic shear mode with propagation vector $\vec{q}||[110]$ and displacement vector $\vec{e}||[1\bar{1}0]$.[3] At the transition temperature $T_M = 46°K$, the crystal structure changes from cubic to a slightly distorted tetragonal structure.[4] Fig. 1 summarizes the frequency shifts seen

*Work performed under the auspices of the U. S. Atomic Energy Commission and NATO Research Grant.

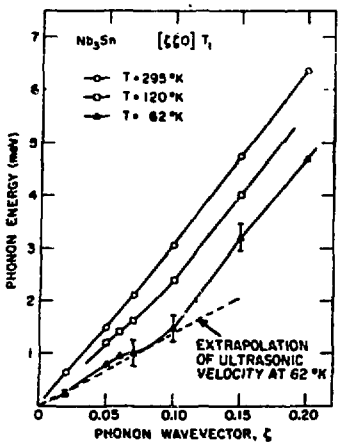

Neg.# 4-675-73

Figure 1. Temperature dependent transverse acoustic phonon dispersion at small wave vectors propagating in the "soft" [110] direction in Nb_3Sn.

in these soft [ζζ0] TA phonons as the temperature is lowered toward T_M. It is probable that the change in slope which occurs at $q \sim 0.1$ is related to the change in screening which occurs as the phonon wave vector passes through parallel edges of the Fermi surface. Most interesting for the purposes of the present discussion are the changes in the power spectrum of the soft phonons in the range of wave vector shown in Fig. 1 as the temperature is lowered further. Typical of these observations are the data in Fig. 2 showing that as the temperature is lowered there is a gradual evolution of a central component in the scattering spectrum in addition to the familiar "phonon-like" sidebands. Although the sideband structure continues to move to lower frequencies as the temperature is lowered, far more dramatic (note the logarithmic scale) is the growth of intensity of the central component which completely dominates the fluctuation spectrum near T_M. The apparent width of the central component can be essentially accounted for by the resolution of the instrument alone. Thus the intrinsic width which adds in quadrature to the instrumental width is small, 1/3 or less of the observed width. Fig. 3 demonstrates that this central peak intensity maximizes at or very near T_M and thus represents the major contribution to the critical scattering associated with the structural transformation. An additional qualitative observation is that although this additional central component can be observed at least out to $q = 0.1$, its

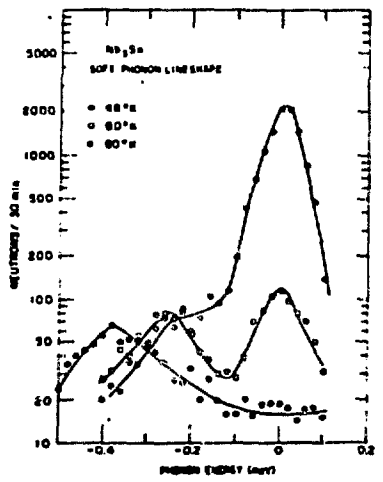

Neg. # 4-676-73

Figure 2. Observed spectral profiles of [ζζ0] T_1 phonon mode in Nb_3Sn with $\zeta \approx 0.02a^*$ at several temperatures above T_M. Only the phonon annihilation portion of the spectrum is shown. The data were taken with an incoming neutron energy of 5 meV and the energy resolution is ∿ 0.1 meV.

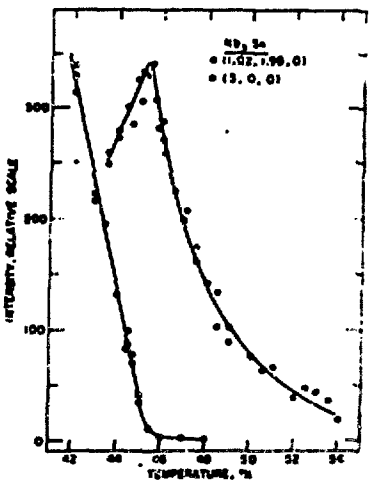

Neg.# 8-126-71

Figure 3. The closed circles show the onset of the structural phase transformation as monitored by the "forbidden" (300) Bragg reflection. The open circles represent the temperature dependence of the central component in the neutron critical scattering spectrum of Nb_3Sn.

presence is restricted to propagation directions nearly along the soft [110] direction. Finally, by observing this feature for several values of momentum transfer $\vec{Q} = \vec{G} + \vec{q}$ which differed by only a reciprocal lattice vector $\vec{G}$, we found the intensities of the central component and the phonon sidebands to be in a constant ratio. This seems to establish that both the central peak and the sidebands are describing the motion of one and the same mode, but that the mode dynamics are characterized by both the normal phonon-like oscillatory response and some slower response as well. (I will discuss later the still-to-be-eliminated possibility that the central component is a purely static phenomenon.)

In order to discuss our observations in a quantitative way, it was necessary to invent some kind of a theoretical construction, however tentative, and this we did in the following way. Quite generally, the frequency dependent part of the one-phonon scattering cross section may be written as

$$S(\omega) = \left(\frac{k_B T}{\hbar\omega}\right) \mathrm{Im}\{\omega_0^2 - \omega^2 - i\omega\Gamma(\omega)\}^{-1} \qquad (1)$$

where ω_0 is a temperature-dependent quasiharmonic frequency and we assume $k_B T >> \hbar\omega$ for the frequency range of interest. Soft-mode line shapes have previously been discussed in the "viscous damping" approximation in which Γ is taken to be a frequency-independent constant. The condition for dynamical instability, $\omega_0 \to 0$, is connected with the divergence of the integrated scattering intensity $I(\text{total}) = \int S(\omega)d\omega \propto \omega_0^{-2}$. This form leads to either a two- or one-peaked function, depending upon the ratio Γ/ω_0, and is not capable of explaining even qualitatively the profiles shown in Fig. 2.

In general, however, Γ itself has a frequency dependence which reflects the changing density of excitations with which the one-phonon state can interact. Sufficiently large changes in $\Gamma(\omega)$ in the important frequency region near ω_0 can produce more complicated spectral profiles. We postulated the following simple form for the phonon self-energy function

$$\Gamma(\omega) = \Gamma_0 + \delta^2/(\gamma - i\omega). \qquad (2)$$

Schwabl later independently proposed a similar Ansatz for $\Gamma(\omega)$ in discussing the central mode in $SrTiO_3$.[5] We imagined the first term in Eq. (1) to represent the normal damping due to phonon-phonon scattering and the second term as due to coupling with another (as yet unspecified) fluctuation with a Debye relaxation spectrum. Eq. (1) has been criticized on the grounds that it violates certain moment sum rules. This is related to the failure of $\Gamma(\omega) \to 0$ as $\omega \to \infty$. Γ_0 should be thought of as the low

frequency approximation to a function $\Gamma_0(\omega)$ which varies slowly over the region $\omega \lesssim \omega_0 << \omega_D$, where ω_D is the Debye frequency of the solid. Thus in systems studied thus far it is mathematically correct but physically improper to omit Γ_0 in Eq. (1) on the basis that the remaining term satisfies higher moment sum rules.

Eq. (1) seems now to be established as the canonical line shape in the central mode problem. One would do well to remember however that it has a very slender foundation in microscopic theory. It has survived rather well whatever experimental tests we have subjected it to, but these have not been stringent enough to allow us to say that a correct theory must yield this exact analytical form.

Inserting Eq. (2) into Eq. (1) gives

$$S(\omega) = \left(\frac{k_B T}{\pi}\right) \frac{\left[\Gamma_0 + \frac{\delta^2 \gamma}{\omega^2+\gamma^2}\right]}{\left[\left(\omega_\infty^2 - \frac{\delta^2\gamma^2}{\omega^2+\gamma^2} - \omega^2\right)^2 + \omega^2\left(\Gamma_0 + \frac{\delta^2\gamma^2}{\omega^2+\gamma^2}\right)^2\right]} \tag{3}$$

where $\omega_\infty^2 = \omega_0^2 + \delta^2$. This formula has the general qualitative features of Fig. 2. In the limit $\omega_\infty^2 >> \delta^2$, it shows three distinct peaks with side bands at $\pm\omega_\infty$. In the other limit $\omega_0 \to 0$ (i.e. $\omega_\infty \to |\delta|$), Eq. (3) shows a profile with shoulders similar to that observed in Fig. 2 at 46°K.

For a more quantitative comparison with experiment, we can conveniently divide the cross section into $S(\omega)_{total} = S(\omega)_{central} + S(\omega)_{sideband}$ with

$$S(\omega)_{central} = \left(\frac{k_B T}{\pi}\right)\left(\frac{\delta^2}{\omega_0^2\omega_\infty^2}\right)\left(\frac{\gamma'}{\omega^2+\gamma'^2}\right) \tag{4}$$

where $\gamma' = (\omega_0^2/\omega_\infty^2)\gamma$. This formula is valid for the range of parameters of interest, $\omega_\infty >> \gamma$ and $\Gamma_0 << (\delta^2/\gamma)$. As with the simpler damping, $I_{total} \propto \omega_0^{-2}$ and dynamical instability occurs as $\omega_0 \to 0$. The fractional integrated central peak intensity is simply

$$\frac{I(central)}{I(total)} = \frac{\delta^2}{\omega_\infty^2} . \tag{5}$$

From data of the type shown in Fig. 1, it is straightforward to obtain both the ratio I(central)/I(total) and the value of ω_∞ (essentially the peak of the phonon sideband), so that Eq. (5)

can be used to deduce a value of $|\delta|$. Investigation for various wave vectors establishes that $|\delta|$ varies approximately linearly with q, $|\delta| = \lambda q$. The principal prediction of this phenomenological theory is that the central mode intensity grows not in proportion to the increasing intensity of the soft phonon sidebands ($\sim T/\omega_\infty^2$) but rather at the much faster rate ($\sim T\delta^2/\omega_\infty^2\omega_0^2$). The observed temperature dependence is consistent with this relation if δ is taken as temperature independent.

There is one additional initially puzzling feature of our data which is resolved by our present understanding of the significance of the central mode. At room temperature the value of the $(\zeta\zeta 0)T_1$ phonon velocity derived from neutron measurements is essentially equal to that obtained by ultrasonic techniques[3]. However, as shown in Fig. 4 there is an increasing systematic discrepancy between the two types of measurements. We may suppose that the ultrasonic frequency (40 MHZ in this instance) is negligibly small compared with the inverse relaxation time γ, in which case one measures a low frequency sound velocity v_0. On the other hand, phonon frequencies from which the neutron determined velocity is derived is much greater than γ, in which case the observed phonon velocity can be shown from Eq. (3) to be

$$v_\infty^2 = (\omega_\infty^2/q^2) = v_0^2 + \lambda^2 \qquad (6)$$

Plotted in Fig. 4 are the ultrasonic velocities v_0 and the values of v_∞ calculated from Eq. (6), and using the value $\lambda = 6.42 \times 10^4$ cm/sec obtained from the above analysis of the central peak amplitude. v_∞ agrees very well with the velocities obtained from the direct analysis of the sideband frequencies obtained from the

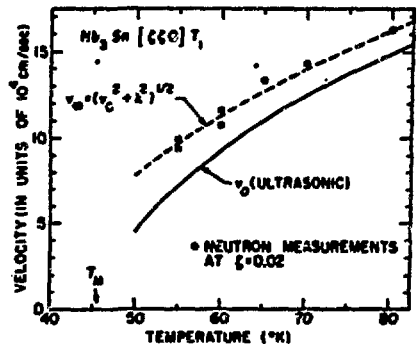

Neg. # 6-182-72

Figure 4. The $(\zeta\zeta 0)T_1$ phonon velocity in Nb_3Sn determined by neutron scattering differs from ultrasonic velocities by an amount which is predictable from the amplitude of the central component.

neutron experiments.

$SrTiO_3$

As is now well known, the structural phase transformation in $SrTiO_3$ at ~105°K results from the instability of a zone boundary phonon.[7-9] In the cubic phase the displacements of the soft mode transform according to the triply degenerate R_{25} representation of the group of R and correspond to rotation of the oxygen tetrahedra about the <100> axes. At T_c there is a doubling of the unit cell and the zone boundary of the cubic phase now becomes the zone center of the tetragonal phase. The triply degenerate zone-boundary R_{25} mode of the cubic phase splits into two zone-center modes: a doublet with rotation axes perpendicular to the fourfold axis and a singlet with rotation axis parallel to the fourfold axis. Subsequent to the discovery of the "central mode" in $SrTiO_3$ by Riste et al further experiments were carried out in collaboration with Riste at the HFBR at Brookhaven.[10]

In the study of Nb_3Sn the small sample size (0.05 cm^3) severely limited the scope of the study, but fortunately the extension of the central component in reciprocal space was much larger than the corresponding q-width of the instrumental resolution. While the observed line shapes were still subject to considerable correction for finite energy resolution, to within a reasonable first approximation the relative integrated intensities of the central and sideband components were given directly from the experimental data. In the case of $SrTiO_3$ (as well as $KMnF_3$ and $LaAlO_3$, to be discussed later) the cross section was observed to vary rapidly over a range of q comparable to the instrumental width. This necessitated resolution corrections, the importance of which can be visualized with the aid of Fig. 5, which schematically shows a cross section corresponding to a phonon dispersion surface, some additional cross section around $\omega=0$, and the resolution ellipse drawn to scale for a typical high resolution experiment. A constant Q scan moves the resolution function parallel to the energy axis through the scattering cross section. For a particular setting $(\vec{Q}_s,\omega_s)$ of the spectrometer the observed neutron intensity is

$$I(\vec{Q}_s,\omega_s) = \int d\vec{Q}d\omega R(\vec{Q}-\vec{Q}_s,\omega-\omega_s)\sigma(\vec{Q},\omega) \qquad (7)$$

and

$$\sigma(\vec{Q},\omega) = \frac{k_F}{k_I} |F_{in}(\vec{Q})|^2 S_{\vec{q}}(\omega) \qquad (8)$$

where k_F and k_I are the final and initial neutron momenta and

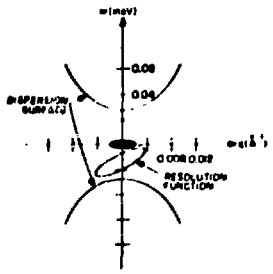

Neg. # 3-233-72

Figure 5. Schematic representation of a cross section of the soft phonon dispersion near the R-point in $SrTiO_3$, with additional scattering near ω=0. The resolution ellipse is drawn to scale for 5-meV incident neutron energy, 20' horizontal collimation.

$F_{1n}(\vec{Q})$ is the inelastic structure factor for the mode with a reduced momentum $\vec{q} = \vec{Q} - \vec{G}$.

The intensity of the phonon-like sidebands changes with $\vec{Q}$ much less rapidly than does that of the central component, the two components are therefore weighted differently by the spectrometer. The proper resolution correction can be applied only if we know the Q dependence of $\sigma(\vec{Q},\omega)$. If the dynamical matrix is expanded about $\vec{q}_R = (1/2,1/2,1/2)$, the behavior of the "bare" phonon modes near $\vec{q}_R$ are determined by a truncated dynamical matrix[11]

$$\underline{C}_T(\vec{q}) = \omega_o^2(\vec{q}_R)\underline{1} + (\vec{q}-\vec{q}_R)\cdot\underline{\lambda}\cdot(\vec{q}-\vec{q}_R) \qquad (9)$$

where $\underline{1}$ is a 3x3 unit matrix and $\underline{\lambda}$ contains the 3 independent constants which can be adjusted to agree with the measured frequencies $\omega_o^2(\vec{q})$. The inelastic structure factors $F_{1n}(\vec{Q})$ are easily evaluated from the eigenvalues of Eq. (9). Although we can safely neglect the q-dependence of Γ_o, our phenomenological derivation of $S_q(\omega)$ gives us no guide for predicting $\delta(\vec{q})$ and $\gamma(\vec{q})$. Our analysis will be independent of any detailed assumptions about $\gamma(\vec{q})$, but in setting $\delta(\vec{q})$ = constant, we are in effect averaging whatever q-dependence there is in this quantity over the sampled region of momentum transfer.

Fig. 6 is an example of the observed line shape at about ten degrees above T_c. Very high resolution was obtained by using low energy (4.9 meV) incident neutrons and higher energy contamination was reduced to a negligible level by a Be filter. The

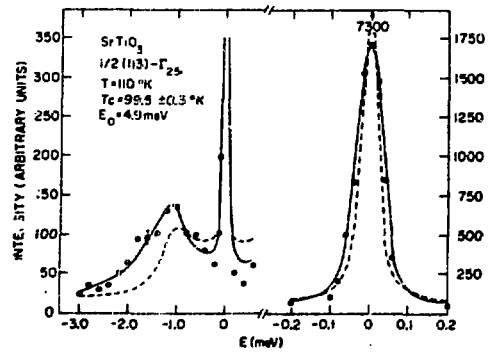

Neg. # 4-187-72

Figure 6. Scattered-neutron spectrum of $SrTiO_3$ at $T \sim 110°K$. The circles are the observed data, the full line represents the fit of the data with Eq. (3) folded with the instrumental resolution; $\Gamma_0 = 0.88 \pm 0.1$ meV, $\delta^2 = 0.63 \pm 0.1$ meV^2, $\omega^2 = 1.27 \pm 0.1$ meV^2, $\lambda_1 = 500$ meV^{2}Å^2, $\lambda_2 = 1000$ meV^{2}Å^2. The dashed curve is a plot of $S(\omega)$ with the above parameters.

incoherent scattering (a small correction at this temperature)was measured separately and has been subtracted. The importance of the resolution corrections, seen by comparing the solid and dotted curves is, as expected, most pronounced on the central peak.

Since the observed linewidth of the central peak was always resolution limited we chose a nominal value of γ' such that it was always smaller than the energy resolution of the spectrometer. After a good fit was obtained γ' was allowed to vary. The fit was insensitive to γ' provided it was smaller than the instrumental resolution and larger than the mesh size required for the numerical folding. As can be seen most easily by the approximate Eq. (4), δ^2 can still be determined accurately under these conditions from the integrated central peak intensity.

Fig. 7 shows the temperature dependence of δ^2, $\omega_\infty^2(\vec{q}_R)$ and $\omega_0^2(\vec{q}_R)$ deduced by fitting many experimental results to Eq. (3). Several internal checks, such as the consistency of parameters obtained with different spectrometer resolution as well as the overall goodness of fit, convince us that the form of the parameterized cross section we have chosen is not grossly inappropriate. There are at least two features here worthy of comment. δ^2 is apparently constant at ~ 0.9 meV^2 for $T - T_c > 25°K$, decreasing to about $0.3(\pm 0.1)$meV^2 at T_c. It is possible, however, that all or part of this apparent T-dependence results from our rather ad hoc assumption that δ^2 is q-independent.

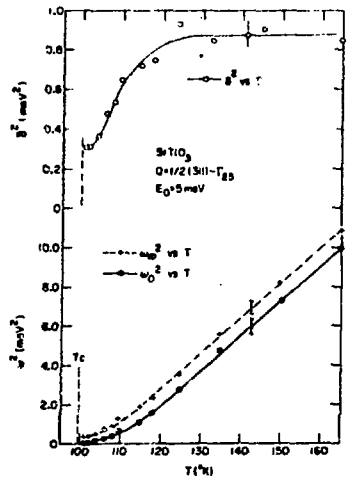

Neg. # 3-240-72

Figure 7. δ^2, ω_∞^2, ω_0^2 vs. T for $SrTiO_3$.

In agreement with previous studies[1,12] ω_∞^2 is essentially linear with temperature in the range $10°K < T - T_c < 180°K$, but a deviation from this simple mean field behavior is clearly evident at lower temperatures for both ω_∞^2 and ω_0^2. Since ω_0^2 is essentially the inverse static susceptibility an attempt was made to deduce a critical exponent, γ, using the relation $\omega_0^2(T \to T_c) \sim (T-T_c)^\gamma$ but the results were not satisfactory, perhaps because of the limited temperature range of our observations. However, our measurements strongly suggest that if such a limiting form is applicable, $1.5 < \gamma < 2.5$. It was not possible to make meaningful measurements nearer T_c because of our inability to determine T_c to better than $\sim \pm 0.5°$. This determination of T_c was made by observing the intensity change of the cubic (222) reflection caused by extinction relief in the strained tetragonal crystal.

$KMnF_3$

$KMnF_3$ exhibits the same cubic-tetragonal transformation that exists in $SrTiO_3$ with $T_c = 186°K$.[13] Gesi et al[14] studied the temperature dependence of the soft mode line shape with moderately high resolution and were able to describe their observations with a simple damped harmonic oscillator response, but found an unexpected temperature dependence of the damping parameter Γ_0. This led us to a reinvestigation of $KMnF_3$ with higher resolution and the observation of a narrow central component in addition to a broader overdamped phonon peak.[10]

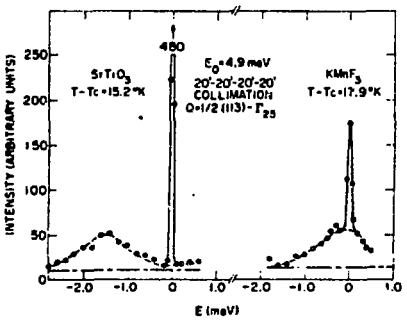

Neg. # 3-238-72

Figure 8. Scattered-neutron spectra of $SrTiO_3$ and $KMnF_3$ at $T-T_c$ = 15.2 and 17.9°K, respectively. The dotted line corresponds to the phonon peak and the solid line to the central component. The dashed line corresponds to level of room background. All incoherent scattering has been subtracted.

Fig, 8 compares the soft phonon line shapes of $SrTiO_3$ and $KMnF_3$ under identical high resolution and at nearly identical values of $T-T_c$. It shows unambiguously the existence of the central peak in $KMnF_3$ as well as in $SrTiO_3$. In the latter, the phonon peak (dotted line) is underdamped, whereas in $KMnF_3$ the phonon is well overdamped at this value of $T-T_c$ and appears as a broad line centered around $\omega=0$. Sitting on top of this broad line is the narrow central peak. In addition, the linewidth of the central peak in both systems is that of the instrumental resolution. This sets an upper limit on the value of the central component: $\gamma < 0.02$ meV ($=0.16$ cm^{-1} $= 4.8 \times 10^9$ Hz).

Although there is no difficulty in fitting the line shape observed in $KMnF_3$ to Eq. (3), the results are considerably less reliable because severe correlations develop between the fitting parameters, particularly ω_∞^2 and δ^2. If, however, we use the values of $\omega_\infty^2(T)$ given by Gesi et al (which should be reasonably reliable for T not too close to T_c) values of $\delta^2 \sim 0.3 \pm 0.1$ meV^2 can be estimated.

If, in accordance with our assumption that $\delta(\vec{q})$ can be regarded as $\vec{q}$-independent, the central mode intensity depends upon $\vec{q}$ only through $\omega_\infty(\vec{q})$, and from Eq. (4), it is given approximately by $[\omega_\infty^2(\vec{q})\omega_0^2(\vec{q})]^{-1}$. $\omega_\infty^2(\vec{q})$ is much more anisotropic in $KMnF_3$, the soft branch being especially low along the Brillouin zone boundary from R(1/2 1/2 1/2) to M(1/2 1/2 0). We should therefore expect the central mode intensity to be more diffuse in $KMnF_3$, extending especially in the direction R → M. This indeed appears to be the case.

$LaAlO_3$

This perovskite material also has (1/2 1/2 1/2) wave vector phonon instability[14], but the rotation of the anion octahedra is about (111) axes rather than about (100) as is the case for $SrTiO_3$ and $KMnF_3$. A recent reexamination of the soft mode line shape by Kjems et al[15] establishes the existence of a central peak in this material as well. The damping of the phonon-like sidebands, although greater than for $SrTiO_3$, was not found to be as large as in $KMnF_3$, and made possible a more extensive quantitative discussion. The collection and treatment of the experimental data was very similar to that for $SrTiO_3$. The energy width was resolution limited, with an upper limit of $\gamma' \leq 0.03$meV. Eq. (3) adequately represented the observed scattering and for $T-T_c \geq 15°C$, $\delta^2 = 0.38 \pm 0.1$ meV^2 and was nearly temperature independent. As was the case in $SrTiO_3$, ω^2 and ω_∞^2 exhibited linear temperature dependence well away from T_c but the extrapolated values go to zero well above the observed transformation temperature, and the observed frequencies deviate considerably from the mean field behavior near T_c. The behavior of both $\omega_\infty^2(T)$ and $\delta^2(T)$ are shown in Fig. 9. The central component showed a clearly resolvable q-width which agreed well with that predicted by the q-dependence of ω_∞^2.

DISCUSSION

From the outset we have assumed that the scattering associated with the central mode is a part of the one-phonon response and is dynamical in nature, but with a narrow frequency response. However, in view of the fact that we have not succeeded in demonstrating experimentally an energy width, it is important to

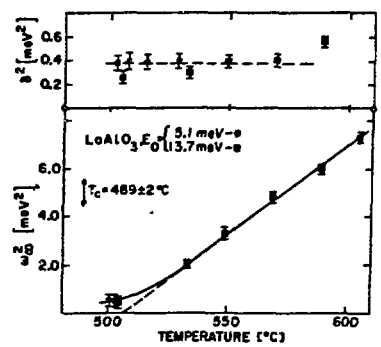

Neg. # 2-346-73

Figure 9. δ^2 and ω_∞^2 vs T for $LaAlO_3$.

consider whether an alternative static mechanism could explain our observed central component. While it is true that the intensity of the central component near T_M strongly suggests its dynamical origin, it is possible to imagine a plausible and somewhat trivial nondynamical mechanism involving scattering from static strain fields, which is at least in qualitative agreement with many of our observations. It is well known that point defects in a lattice will in general give rise to displacements of neighboring atoms from their equilibrium positions in the homogeneous impurity free crystal. These displacement fields cause diffuse scattering of x-rays or neutrons sometimes known as Huang scattering. The magnitude of the displacement field about an impurity is calculated as a linear response to a force field $\vec{F}(\vec{r})$ which the impurity exerts on the undisplaced lattice. For our purposes it is convenient to Fourier transform the resulting displacements and express them in terms of a linear combination of phonon modes with wave vector q and branch index j. The amplitude of this impurity induced set of static phonon-like displacements is easily shown in the harmonic approximation to be given by

$$\langle Q_{qj} \rangle_{\text{static}} = F_{qj}/\omega_{qj}^2$$

where

$$F_{qj} = -N^{-\frac{1}{2}} \sum_{\ell k} M_k^{-\frac{1}{2}} \vec{F}_{\ell k} \cdot \vec{e}_k^{*}(qj) \exp(-i\vec{q}\cdot\vec{\ell})$$

is the projection of $\vec{F}(\vec{r}) \equiv \vec{F}_{\ell k}$ upon the phonon eigenvector $\vec{e}(q,j)$. The intensity of this static diffuse scattering can be calculated from the corresponding expression for the integrated phonon scattering under the same conditions by simply replacing $\langle Q_{qj}^2 \rangle_{\text{thermal}}$ by $|\langle Q_{qj} \rangle_{\text{static}}|^2$.

$$I_{qj}(\vec{Q})_{\text{static impurity}} \propto |\langle Q_{qj} \rangle_{\text{static}}|^2 = \frac{|F_{qj}|^2}{\omega_{qj}^4} \quad . \quad (7)$$

In normal materials the major contributions come from long wavelength acoustic modes (because of the weighting by ω_{qj}^{-4}) and the effect of impurity concentrations of $\sim 10^{-2}$ can easily be detected and studied against the thermal diffuse background by x-ray scattering. However, Eq. (7) also suggests that this same factor of ω_{qj}^{-4} would greatly enhance the contribution of any phonon mode whose frequency becomes anomalously small near a structural transformation. If impurities are of the proper symmetry to couple to the soft mode, there will be a central component, static in origin, whose intensity grows more rapidly ($\omega_{\text{soft}}^{-4}$) than that of the collapsing phonon sidebands ($\omega_{\text{soft}}^{-2}$).

In spite of these obvious similarities, we do not believe that this impurity mechanism provides a satisfactory explanation of our observations. Although we have not until now made the distinction, it is clear that it is the low frequency stiffness ω_o^2 which goes into Eq. (7) not ω_∞^2, if there is a difference between the two quantities. However, the static impurity mechanism acting alone provides no frequency dependent terms to the phonon self-energy, so that $\omega_o^2 = \omega_\infty^2$ and $I(Q)_{static} \propto 1/\omega_\infty^4$. For Nb_3Sn our measurements closely follow $(1/\omega_o^2\omega_\infty^2)$, and there is a substantial difference between the two predictions especially near T_M. Simply put, ω_∞^2 (as obtained from the phonon sidebands) saturates near T_M while the central intensity continues to increase. Also the observed agreement with the discrepancy between the extrapolated long wavelength acoustic velocities and our measurements and the magnitude of the central component would be entirely fortuitous for this (or for that matter any other) static description of the central component.

We believe that it is unlikely that the impurity effect outlined above is the dominant one in the observations described here. On the other hand, it is certainly a plausible mechanism for producing unusual line shape effects near phonon instabilities and as such deserves further consideration. It is obvious from these comments that it is most important to try to characterize, directly if possible, the energy width of the central component. If the estimate of $\gamma \gtrsim 10^{10}$Hz($\sim$0.4 meV) obtained[16] indirectly from ESR data in $SrTiO_3$ is correct, these widths are at the limit of conventional neutron resolution, and it is possible that light scattering is the more appropriate tool.

REFERENCES

1. T. Riste, E. J. Samuelsen, and K. Otnes in "Structural Phase Transitions and Soft Modes," ed. E. J. Samuelsen, E. Andersen, and J. Feder (Universtetsforlaget, Oslo, Norway, 1971). See also, T. Riste, E. J. Samuelsen, K. Otnes, and J. Feder, Solid State Commun. 9, 1455 (1971).

2. G. Shirane and J. D. Axe, Phys. Rev. Letters 27, 1803(1971).

3. W. Rehwald, M. Rayl, R. W. Cohen, and G. D. Cody, Phys. Rev. (to be published). This contains references to earlier work.

4. R. Mailfort, B. W. Batterman, and J. J. Hanak, Phys. Lett. 24A, 315 (1967); L. J. Vieland, R. W. Cohen, and W. Rehwald, Phys. Rev. Letters 26, 373 (1971).

5. F. Schwabl, Phys. Rev. Letters 28, 500 (1972).

6. T. Schneider, to be published.

7. H. Unoki and T. Sakudo, J. Phys. Soc. Japan 23, 546 (1969).

8. P. A. Fleury, J. F. Scott, and J. M. Worlock, Phys. Rev. Letters 21, 15 (1968).

9. G. Shirane and Y. Yamada, Phys. Rev. 177, 858 (1969).

10. S. M. Shapiro, J. D. Axe, G. Shirane, and T. Riste, Phys. Rev. B 6, 4332 (1972).

11. K. Gesi, J. D. Axe, and G. Shirane, Phys. Rev. B 5, 1933 (1972).

12. K. Otnes, T. Riste, G. Shirane, and J. Feder, Solid State Commun. 9, 1103 (1971).

13. V. J. Minkiewicz and G. Shirane, J. Phys. Soc. Japan 26, 674 (1969); G. Shirane, V. J. Minkiewicz, and A. Linz, Solid State Commun. 8, 1941 (1970).

14. W. Cochran and A. Zia, Phys. Stat. Sol. 25, 273 (1968); G. Shirane, and K. A. Müller, Phys. Rev. 183, 820 (1969).

15. J. K. Kjems, G. Shirane, K. A. Müller, and H. J. Scheel, to be published.

16. Th. von Waldkirch, K. A. Müller, and W. Berlinger, Phys. Rev. B 7, 1052 (1973).